Modeling Flight Delay Propagation: A New Analytical-Econometric Approach

Nabin Kafle, Bo Zou

Department of Civil and Materials Engineering, University of Illinois at Chicago, Chicago, IL 60607, United States

Abstract: Flight delay presents a widespread phenomenon in the air transportation system, costing billions of dollars every year. Some delay originating from an upstream flight spreads to downstream flights. This phenomenon is defined as delay propagation. To understand the delay propagation patterns and associated mitigation measures, this study proposes a novel analytical-econometric approach. Considering that airlines deliberately insert buffer into flight schedules and ground turnaround operations, an analytical model is developed to quantify propagated and newly formed delays that occur to each sequence of flights that an aircraft flies in a day, from three perspectives on the ways that delays are absorbed by the buffer. With delays computed from the analytical model, we further develop a joint discrete-continuous econometric model and use the Heckman's two-step procedure to reveal the effects of various influencing factors on the initiation and progression of propagated delays. Results from the econometric analysis provide estimates on how much propagated delay will be generated out of each minute of newly formed delay, for the US domestic aviation system as well as for individual major airports and airlines. The impacts of various factors on the initiation and progression of propagated delay are quantified. These results may help aviation system planners gain additional insights into flight delay propagation patterns and consequently prioritize resource allocation while improving system overall performance. Airlines can also be better informed to assign buffer to their flight schedules to mitigate delay propagation.

Keywords: Propagated delay, Newly formed delay, Flight buffer, Ground buffer, Analytical model, joint discrete-continuous econometric model

1 Introduction

Flight delay is a major challenge facing the air transportation system today. In the US, total flight delay cost is estimated to be over $30 billion each year (Ball et al., 2010). The cost comes from various sources, including additional use of crew, fuel, and aircraft maintenance; increase in passenger travel time; greater environmental externalities; and the macroeconomic impact of flight delay on other economic sectors. While solutions such as improvement in air traffic management (e.g., Ball et al., 2007; Swaroop et al., 2012) and aviation infrastructure investment (Zou and Hansen, 2012a; Zou, 2012) are expected to substantially reduce flight delays, an important means from the airlines' perspective is to judiciously schedule flights. Specifically, by inserting additional times than the minimum necessary in and between flights, unexpected delays can be absorbed and consequently their propagation to downstream flights can be mitigated or avoided. The objective of this study is to advance the understanding of the delay propagation patterns and of the ways delays are mitigated by the additional times.

Propagated delay occurs because of connected resources involved in an initially delayed flight and flights downstream. The connected resources can be the aircraft, crew, passengers and airport resources. For example, the same aircraft flies multiple flight legs in a day. Delay of an earlier flight can sustain in the subsequent flights of the same aircraft. Flight crew can also switch between multiple aircraft, causing the delay from one flight to propagate across multiple flights. Connecting passengers at hub airports, like crew members, are also often responsible for the propagation of delay when a connecting flight has to wait for passengers from their previous delayed legs. Overall, delay can grow over the course of a day, with a small initial delay leading to larger delays later in the day. To mitigate this propagation effect, additional times are inserted in both flight schedules and ground turnaround operations. In this study, we term these additional times as flight buffer and ground buffer. The buffer can be interpreted as the *ex-ante* amount of time built into a scheduled activity based on an expected amount of time for an activity plus an amount to maintain a level of on-time service. To some extent, it is analogous to an inventory problem.

In the literature, analytical research on flight delay propagation dates back to 1998, when Beatty et al. (1998) used flight schedules of American airlines to calculate delay propagation multipliers. A delay propagation multiplier is a value which when multiplied with the initial delay yields the sum of all potential downstream delays plus the initial delay. Beatty et al. constructed delay trees by considering three causes for delay propagation: aircraft equipment, cockpit crew, and flight attendants. A delay tree can contain up to 50-75 flights for a flight early in the day that is connected to the rest of the system. However, the authors did not show how delays can be absorbed by flight and ground buffers. AhmadBeygi et al. (2008) also constructed tree structure to investigate how delay can propagate throughout an airline's network in a day, for two US airlines. In the delay tree, the root delay, which occurs to the earliest flight in the tree, propagates to immediate downstream flights of the same aircraft. In cases that the cockpit crew and aircraft do not stay together, delay propagates to the flight the cockpit crew heads. Ground buffer was accounted for as a means to mitigate delay propagation. However, propagated delays due to connecting flight attendants or passengers and the delay recovery options were not included in the analysis. Welman et al. (2010) calculated delay multipliers for 51 US airports and estimated the reduction in total system delay if airport capacity was expanded. Buffer was not included while calculating propagated delay. Churchill et al. (2010) developed another analytical model, which explicitly accounts for ground buffers but not flight buffer. A measure for the level of network-wide extension of flight delays was introduced in Fleurquin et al. (2013) to define when an airport is congested and study how congested airports form connected clusters in the network.

Apart from the analytical approaches, other methods were used in flight delay propagation research. Wong and Tsai (2012) considered simultaneously flight and ground buffers and statistically estimated a survival model for flight delay propagation. Xu et al. (2008) used multivariate adaptive regression splines and found on average 5.3 minutes of generated delay and 2.1 minutes of absorbed delay across 34 Operational Evolution Plan (OEP) airports in the US. Pyrgiotis et al. (2013) developed a queuing engine to model flight delay formed at an airport. The formed delay was then utilized to modify the flight schedules

and update demand at the airports. The two processes iterate to obtain the final local delay formed at an airport and its propagation. Most recently, Campanelli et al. (2016) used two agent-based models to simulate flight delay propagation and assessed the effect of disruptions in the US and European aviation networks.

While inserting buffer is an effective means to mitigate delay propagation, doing so has adverse effects. First, buffer makes flight schedules and ground turnaround times longer than the minimum necessary, reducing the utilization of aircraft and incurring greater capital cost. Second, because payment to airline crew is determined in part by the length of flight schedules, inserting flight buffer increases crew expenses. Third, with flight buffer, flights often arrive earlier when there is no delay. The landed aircraft are likely to encounter gate unavailability and thus have to wait in queue on the ramp with engines on, which increases airline operating cost and ramp congestion, and potentially aggravates passengers onboard (Hao and Hansen, 2014). These adverse effects prompt airlines to consider the best tradeoff when setting buffers in their flight schedules. Following this line of thought, AhmadBeygi et al. (2010) investigated the issue of reallocating ground buffer by re-timing flight departures, such that delay propagation can be mitigated without incurring additional planned cost. Monte Carlo simulations were performed in Schellenkens (2011) to establish the relationship between the duration of primary delays and the number of affected downstream flights. Focusing on delay propagation, Arikan et al. (2013) proposed several metrics to investigate the robustness of US airline schedules, and showed different airline strategies in setting flight and ground buffers.

Despite these efforts for modeling propagated flight delay, two important methodological gaps exist. First, no studies have so far looked into simultaneous use of flight and ground buffers in absorbing both propagated and newly formed delays. At a given flight arrival or departure point (or node, as we define in the next section), newly formed delay is defined as the delay that occurs during the immediate upstream operation (which can be either a flight or a ground turnaround); whereas propagated delay is delay that is rooted further upstream. Among the aforementioned studies, Churchill et al. (2010) and Arikan et al. (2013) considered only ground buffer. Although both flight and ground buffers were modeled in Schellenkens (2011), the authors did not differentiate between newly formed and propagated delays, nor the way the two types of delays are absorbed by buffer. In fact, there is no way to get specific empirical data on the two types of delays. Yet with the coexistence of propagated and newly formed delays, buffer could be used to first absorb newly formed delay and then propagated delay, or vice versa, or both at the same time. To fill this gap, the present study explicitly investigates three scenarios in which propagated and newly formed delays are distinguished and absorbed by flight and ground buffers.

The second gap in the literature is a lack of statistical evidence of under what conditions newly formed delay will propagate downstream and, provided that it occurs, how the delay propagation is shaped by subsequent ground and flight buffers and the macro-congestion environment. Such statistical evidence is important to better understanding delay propagation patterns and mitigation strategies and build schedules that are more robust to delays. In view of this gap, the present study makes a second contribution by proposing a joint discrete-continuous econometric model for the initiation and progression of propagated flight delay. The model consists of a latent variable based discrete choice model for propagated delay initiation and a regression model for the progression of propagated delay. Because flights that initiates propagated delays are not *randomly* pick from the population of flights, our estimation explicitly accounts for potential bias due to sample selection. Both a sequential and a simultaneous methods are used to obtain consistent model estimates. The contribution of initial delays, delay mitigating measures, and macro-congestion environment to delay propagation is statistically quantified, to our knowledge the first time in the literature. The estimates further allow us to infer the vulnerability to delay propagation at individual airports and for different airlines. We also discuss how these estimates can be useful to aviation system planners and airlines.

The remainder of the paper is organized as follow. Section 2 offers formal (although still conceptual) definitions for propagated and newly formed delays and the way delays buffer absorbs them. Section 3 describes the analytical model for computing the two types of delays under three scenarios, which provide

bound estimates of propagated delay and represent different sets of assumptions that can be made to produce useful results. An application of the analytical model to the US domestic air transportation system is subsequently presented. In Section 4, we present a joint discrete-continuous model to empirically characterize the initiation and progression of propagated delays, including model specification, estimation methods, discussion of results and their implications. Summary of findings is offered in Section 5.

2 Newly formed and propagated delays

Before quantifying delay and buffer, it is necessary to characterize the air transportation network. In this study we consider an air transportation network as a graph consisting of nodes and links. The node-link representation of air transportation networks is not new in the literature. Guimera et al. (2005) and Barrat et al. (2004) used graphs to characterize air transportation networks in which nodes are airports and links are direct flights between the nodes. Our definition of nodes and links is somewhat different: each node corresponds to either an *actual* gate push-back or an *actual* gate arrival of a flight. Thus a node is associated with an airport. A link connects two neighboring nodes (time wise). A link can be either a flight or a ground turnaround. To illustrate, Figure 1 shows the nodes and links of an aircraft's itinerary in a time-space diagram. The aircraft flies three flights. Consequently the total number of nodes is six, one for each takeoff or landing. The time next to each node is the actual departure/arrival time (in standard time (e.g., Eastern Standard Time)) at the node, and the numbers next to the arrows indicate the flight delays at the nodes.

In this study, newly formed delay at a node refers to delay that occurs between the node and its immediate upstream node. For example, in Figure 1 the departure delay at DEN is 20 minutes. Since it is the beginning of the aircraft's operation, all 20 minutes are newly formed delay at the DEN node. Between the DEN and DFW nodes (i.e., while the aircraft is flying), some newly formed delay must occur, as the arrival delay at DFW increases to 25 minutes. The newly formed delay will be counted at the DFW node. Newly formed delay can be caused by airport/airspace capacity constraints, aircraft breakdown and maintenance, airport security, etc. In contrast, propagated delay at a node refers to the part of delay that is rooted in some newly formed delay which occurs to the same aircraft but further upstream. Note that in principle delay can propagate between flight segments operated by the same aircraft, but can also propagate from one aircraft to another. One situation in the latter case is that delay of an aircraft during ground turnaround may spill over to an adjacent aircraft at the airport even if the latter arrived at the airport on time, due to shared use of airport resources (e.g. personnel to handle turnarounds). However, since the focus of this paper is on aircraft-specific delay propagation, such inter-aircraft propagated delay will be considered as newly formed delay for the adjacent aircraft.

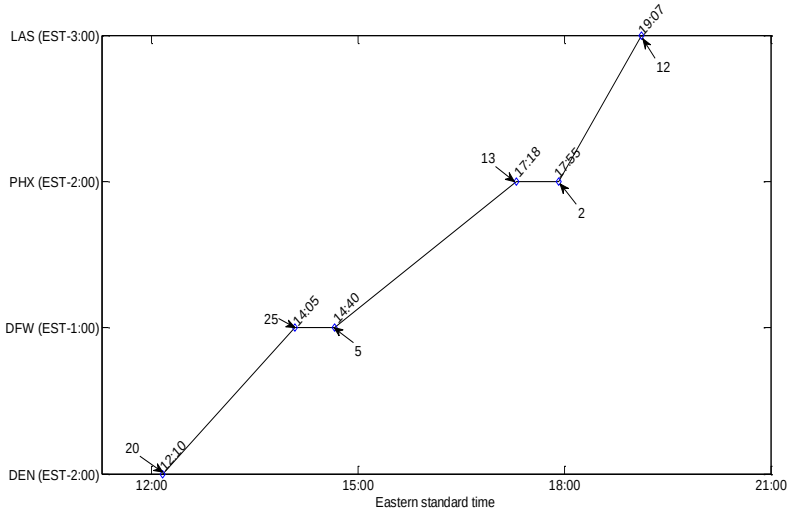

Figure 1: Illustration of link-node representation of aircraft itineraries

In the US domestic air transportation system, actual flight departure/arrival times and delays are all reported to the Federal Aviation Administration (FAA) and made publically available on the Bureau of Transportation Statistics (BTS) website. On the other hand, the distinction between newly formed and propagated delays is not readily made, due to at least two reasons. First, buffers are an artificial construct used to represent the difference between expected and scheduled flight (and ground turnaround) times. Given this and the stochastic nature of actual flight times, there is no universally accepted way to empirically observe or calculate buffers. In this study we have developed several distinct sets of assumptions that we use to calculate the length of buffers. Second, it is uncertain how buffer inserted on a link is used to absorb newly formed delay and propagated delay. As mentioned in Section 1, it can be that buffer first absorbs propagated delay and then newly formed delay, or vice versa, or absorbs both at the same time. Given this uncertainty, we consider below three scenarios for delay absorption. In the first scenario, buffer is used to first absorb propagated delay. Any remaining buffer will be used to reduce newly formed delay. In the second scenario, the absorption order is reversed. In the third scenario, no priority is given while absorbing the two types of delays, i.e., buffer reduces both delays simultaneously.

3 The analytical model

3.1 Computing flight and ground buffers

The analytical model for computing propagated and newly formed delays requires identifying the amount of buffer inserted in flight and ground turnaround schedules. Because the exact amount of buffer is unknown, we consider alternative values for flight and ground buffers. Specifically, we use 5th, 10th, and 20th percentile values of the actual gate-to-gate travel times among flights with departure delay as the plausible nominal flight times, for each combination of flight segment, airline, aircraft category, and season.[1] We consider only flights with departure delay, as these flights clearly have more incentive to fly as efficiently in order to catch up with the schedule. Not choosing the absolute minimum actual time makes the calculation more robust to measurement error, and reduces the influence of unusually favorable conditions, such as strong tailwinds (Zou and Hansen, 2012b). Similarly, we use 25th, 50th, and 75th percentile values of actual ground turnaround times among flights with arrival delay as the plausible nominal times for ground turnaround, for each combination of airline, aircraft category, and season. Considering different percentile values allows us to gauge the robustness and sensitivity of the results.

Once the nominal times for the flight and ground turnaround are obtained, we calculate flight and ground buffers as follows. Consider that the trajectory of an aircraft in a day cover nodes $i = 1,2,\dots,I$. I must be an even number as each flight involves a departure node and an arrival node. Let $U^F_{i-1,i}, \forall i = 2,4,\dots,I$ and $U^G_{i-1,i}, \forall i = 3,5,\dots,I-1$ denote the nominal times for the flight and ground turnaround for the respective link $(i, i-1)$. Consequently the buffer on a flight link is:

$$B_{i-1,i} = \max\left[0, (t^s_i - t^s_{i-1}) - U^F_{i-1,i}\right], \forall i = 2,4,\dots,I \quad (1)$$

The buffer on a ground turnaround link is:

$$B_{i-1,i} = \max\left[0, (t^s_i - t^s_{i-1}) - U^G_{i-1,i}\right], \forall i = 3,5,\dots,I-1 \quad (2)$$

where $B_{i-1,i}$ is the buffer on link $(i-1, i)$; t^s_i is the scheduled departure (or arrival) time of the aircraft at node i. Note that buffers in (1) and (2) are truncated below zero if the scheduled time is less than the nominal time, because buffer can never be negative (i.e., nominal operations cannot be delayed).

[1] In this study we group aircraft into two categories: wide body and narrow body jets. Operations by regional jets and turboprops are not observed for the airlines studied (in fact, such aircraft are operated by the subsidiaries of the airlines studied. See for example, Zou et al. (2014)).

3.2 Computing propagated and newly formed delays

With flight and ground buffers calculated, now we proceed to computing propagated and newly formed delays. Recall that three scenarios may be possible as to how buffer is used to absorb the two types of delays. Below we detail the methodologies for the three scenarios. Although the description is based on flight links, the methodologies apply in a similar way to computing delays on ground links.

We use a simple time-space graph to represent a flight in Figure 2. The horizontal line denotes time and the vertical line represents space. The flight is scheduled to depart from node $i-1$ at t_{i-1}^s and arrive at node i at t_i^s. The amount of flight buffer on link $(i-1, i)$ is $B_{i-1,i}$. If there were no departure delay at node $i-1$ and flying from $i-1$ to i is also free from any en-route delay, then the arrival time of the flight at node i would be earlier than t_i^s by $B_{i-1,i}$. In Figure 2, however, the flight departs late by O_{i-1} (note that O_{i-1} can be a mix of newly formed delay at node $i-1$ and propagated delay from the upstream of node $i-1$).[2] With this departure delay, the best arrival time at node i would be bt_i^a if the aircraft flies nominal time, with an amount of $B_{i-1,i}$ departure delay absorbed by flight buffer on link $(i-1, i)$. The t_i^n represents the normal arrival time at node i given the initial departure delay, which is equal to actual departure time plus scheduled flight length. If a newly formed delay further occurs while the aircraft flies from $i-1$ to i, a late arrival such as t_i^a in Figure 2 would result. The observed delay at each node is the difference between scheduled arrival (departure) and actual arrival (departure) time. Decomposition of this observed delay into newly formed and propagated delay is discussed based on three scenarios.

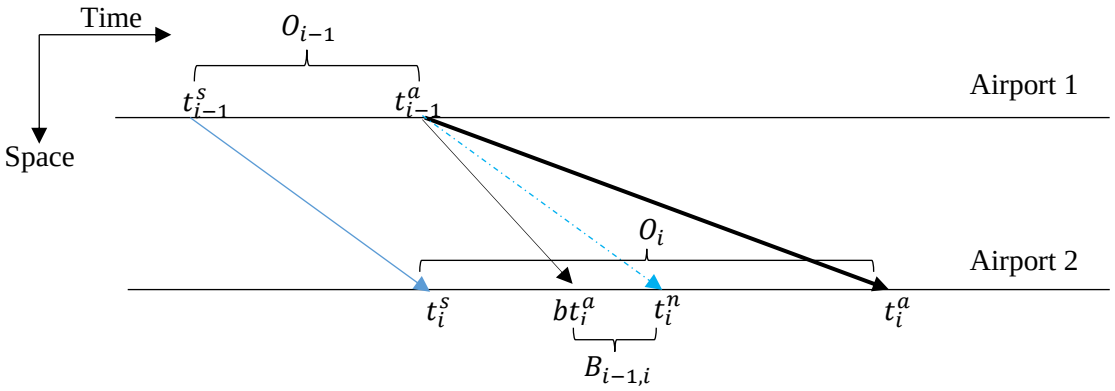

Figure 2: Time-space graph of a single flight

Scenario 1:

Scenario 1 postulates that buffer first absorbs newly formed delay. After newly formed delay is entirely eliminated, any remaining buffer absorbs propagated delay. Referring to Figure 2, if the observed delay at node i is greater than at node $i-1$, i.e., $O_i > O_{i-1}$, it means that some newly formed delay is added to node i even after buffer $B_{i-1,i}$ is used. Because newly formed delay has higher priority over propagated delay for being absorbed, the propagated delay to node i remains O_{i-1}. If $O_i \leq O_{i-1}$, then there is no newly formed delay at node i. Part of the propagated delay from node $i-1$, equaling $O_{i-1} - O_i$, is absorbed by flight buffer $B_{i-1,i}$. We explicate the two cases in Appendix A. Below we present the unified algorithm to calculate the newly formed delay and propagated delay in a recursive manner from the first node of an aircraft in a day. At the first node, the observed delay O_1 is all attributed to newly formed delay N_1.

[2] In this study, we consider observed delays that are truncated below zero, i.e., earlier than scheduled departures (arrivals) will be given zero observed delay values.

Algorithm 1: Computing propagated and newly formed delays under Scenario 1

1. At the first node of an aircraft ($i = 1$), $N_1 = O_1$. There is no propagated delay.

2. For each subsequent node $i = 2, \dots, I$,

2.1. Compute propagated delay whose root is the immediate upstream node $i-1$: $p_{i-1,i} = N_{i-1} * \min(1, \frac{O_i}{O_{i-1}})$;

2.2. Compute propagated delays whose roots are further upstream nodes $k = 1, \dots, i-2$: $p_{k,i} = p_{k,i-1} * \min(1, \frac{O_i}{O_{i-1}})$;

2.3. Compute newly formed delay at node i: $N_i = O_i - \sum_{k=1}^{i-1} p_{k,i}$.

Note that an implicit proportional assumption is made in steps 2.1-2.2. Specifically, buffer used to absorb propagated delays from upstream at node i is allocated proportionately to N_{i-1} and $p_{k,i-1}$ ($k = 1, \dots, i-2$) according to their original amounts. We also apply this assumption in scenarios 2 and 3. Our argument is that—absent empirical evidence—it is unreasonable to justify that buffer prefers to absorb any specific part of upstream propagated delays. An "equal" allocation (i.e., by maintaining their original proportions) seems more plausible. Nonetheless, it may still be interesting to explore alternative ways to allocate buffer, although this is beyond the scope of the present work.

Scenario 2:

Scenario 2 postulates that buffer first absorbs propagated delay. After propagated delay is entirely eliminated, any remaining buffer absorbs newly formed delay. As propagated delay in general has roots at multiple upstream nodes, we again assume that propagated delays rooted in different upstream nodes are absorbed while maintaining their proportions. Newly formed delay at a node is the difference between observed delay and propagated delay. Different from scenario 1, buffer needs to be explicitly involved in delay computation. Depending on the relative length of observed delays between two consecutive nodes and the length of buffer, four cases are possible. We explicate the four cases in Appendix B. Below we present the unified algorithm for the computation of propagated and newly formed delays under the four cases.

Algorithm 2: Computing propagated and newly formed delays under Scenario 2

1. At the first node of an aircraft ($i = 1$), $N_1 = O_1$. There is no propagated delay.

2. For each subsequent node $i = 2, \dots, I$,

2.1. Compute $B^a_{i-1,i} = \max(B_{i-1,i}, O_{i-1} - O_i)$; (see Appendix B for discussion of $B^a_{i-1,i}$.)

2.2. Compute propagated delay from the immediate upstream node $i-1$: $p_{i-1,i} = N_{i-1} * \left[1 - \min(1, \frac{B^a_{i-1,i}}{O_{i-1}})\right]$;

2.3. Compute propagated delay from further upstream nodes $k = 1, \dots, i-2$: $p_{k,i} = p_{k,i-1} * \left[1 - \min(1, \frac{B^a_{i-1,i}}{O_{i-1}})\right]$;

2.4. Compute newly formed delay at node i: $N_i = O_i - \sum_{k=1}^{i-1} p_{k,i}$.

Similar to Algorithm 1, the min operators above allow for differentiating between cases 2(a)/(c) and 2(b)/(d).

Scenario 3:

Scenario 3 postulates that buffer simultaneously reduces newly formed delay and propagated delay in proportion to the share of the two types of delays. The conceptual difficulty here is that the amounts of propagated delay and newly formed delay at a node before buffer absorption are not known *a priori*. However, proportionate absorption suggests that the ratio of propagated to newly formed delays remains constant before and after delay absorption. We let x be the amount of buffer on link $(i-1, i)$ that is used to absorb propagated delay from upstream to node i. Then $B_{i-1,i} - x$ is the amount of buffer on link $(i-1, i)$ that absorbs newly formed delay at node i. The constant ratio requires that:

$$\frac{O_{i-1}}{O_i-(O_{i-1}-x)+(B_{i-1,i}-x)} = \frac{O_{i-1}-x}{O_i-(O_{i-1}-x)} \tag{3}$$

The left hand side (LHS) and right hand side (RHS) of Equation (3) represent the ratios of propagated delay to newly formed delay at node i, without and with the use of buffer respectively. On the LHS, the numerator is the propagated delay (if there were no buffer) to node i, which equals the observed delay at node $i-1$. In the denominator, $O_{i-1} - x$ is the amount of propagated delay after using buffer. Since O_i is the total observed delay, $O_i - (O_{i-1} - x)$ is the amount of newly formed delay with buffer. $O_i - (O_{i-1} - x)$ needs to be added by $B_{i-1,i} - x$, which is the amount of newly formed delay that is absorbed by buffer, to obtain the total newly formed delay absent buffer on link $(i-1, i)$. The LHS should be equal to the ratio of propagated delay and newly formed delay with buffer, i.e., $O_{i-1} - x$ over $O_i - (O_{i-1} - x)$. Solving (3) yields

$$x = \frac{B_{i-1,i}}{B_{i-1,i}+O_i} O_{i-1} \tag{4}$$

Therefore, propagated delay at node i is

$$P_i = O_{i-1} - x = O_{i-1} \frac{O_i}{B_{i-1,i}+O_i} \tag{5}$$

Substituting P_i by $\sum_{k=1}^{i-1} p_{k,i}$ and O_{i-1} by $N_{i-1} + \sum_{k=1}^{i-2} p_{k,i-1}$ gives

$$\sum_{k=1}^{i-1} p_{k,i} = (N_{i-1} + \sum_{k=1}^{i-2} p_{k,i-1}) * \frac{O_i}{B_{i-1,i}+O_i} \tag{6}$$

As in scenarios 1 and 2, we assume that propagated delays rooted in all upstream nodes are absorbed while maintaining their proportions. Then we can decompose propagated delay as follows:

$$p_{i-1,i} = N_{i-1} * \frac{O_i}{B_{i-1,i}+O_i} \tag{7}$$

$$p_{k,i} = p_{k,i-1} * \frac{O_i}{B_{i-1,i}+O_i} \quad \forall k = 1 \dots i-2 \tag{8}$$

Newly formed delay at node i is the difference between observed delay and propagated delay:

$$N_i = O_i - P_i = O_i - O_{i-1} \frac{O_i}{B_{i-1,i}+O_i} = O_i \frac{B_{i-1,i}+O_i-O_{i-1}}{B_{i-1,i}+O_i} \tag{9}$$

Equation (9) holds true for any values of O_{i-1}, O_i and $B_{i-1,i}$, except when $B_{i-1,i} + O_i < O_{i-1}$. This is similar to case 2 (c) (see Appendix B). If this occurs, we adjust the buffer value to $O_{i-1} - O_i$. The implicit assumption by doing this adjustment is that no new delay is formed on link $(i-1, i)$ (as $N_i = 0$ from (9)). Consequently all observed delay at node i (i.e., O_i) is propagated delay.

The above computation of propagated and newly formed delays is summarized by the following algorithm.

Algorithm 3: Computing propagated and newly formed delays under Scenario 3

1. At the first node of an aircraft ($i = 1$), $N_1 = O_1$. There is no propagated delay.

2. For each subsequent node $i = 2, \dots, I$,

2.1. Compute $B^a_{i-1,i} = \max(B_{i-1,i}, O_{i-1} - O_i)$;

2.2. Compute propagated delay from the immediate upstream node $i-1$: $p_{i-1,i} = N_{i-1} * \frac{O_i}{B^a_{i-1,i}+O_i}$;

2.3. Compute propagated delay from further upstream nodes $k = 1, \dots, i-2$: $p_{k,i} = p_{k,i-1} * \frac{O_i}{B^a_{i-1,i}+O_i}$;

2.4. Compute newly formed delay at node i: $N_i = O_i - \sum_{k=1}^{i-1} p_{k,i}$.

So far our discussion has been focused on identifying delays that are propagated to a given node from all upstream nodes. With $p_{k,i}$'s ($\forall k < i$) computed, we can also compute total propagated delay (TPD) rooted in node k to all its downstream nodes, as follows:

$$TPD_k = \sum_{i=k+1}^{I} p_{k,i} \quad \forall k = 1,2, \dots I-1 \tag{10}$$

TPD_k will be the main variable of interests in Section 4.

This concludes the methodologies for computing propagated and newly formed delays at any given node in an air transportation network. Next, we apply the methodologies using historic flight data in the US to obtain insights about delay propagation and formation patterns.

3.3 Data

We use US domestic flight data from eight major carriers (listed in Table 1) in the first quarter of 2007, when the system had one of the worse flight on-time performance records in history. Detailed activity information for each flight is collected from the BTS Airline On-Time Performance database (BTS, 2013a). Based on aircraft model information from the BTS Schedule B-43 inventory database (BTS, 2013b), we group aircraft into two categories: narrow body and wide body. The aircraft model/category information is then merged into the flight operation dataset by matching aircraft tail numbers.

Data filtering is needed to eliminate erroneous recording, such as: (i) teleportation, i.e. an aircraft landed at one airport, but the next departure was from a different airport; and (ii) a flight's departure time was earlier than the arrival time of its previous flight leg. We further remove cancelled and diverted flights, and the associated flights of the same aircraft of the same day. All observations on the transition days between standard and daylight saving times are excluded as these records can be subject to inconsistent recording. After the filtering and conversion process, our final dataset consists of 642,227 observations, covering flights flying between 168 US airports. The total numbers of aircraft from the eight carriers are 2513. Table 1 summarizes the number of flights by airline and aircraft category.

Table 1: Number of flights by airline and aircraft category

Carrier	**Aircraft Categories**		**Total**
	Narrow Body	**Wide Body**	
American	58,038	4,250	62,288
Alaska	28,975	0	28,975
Continental	71,229	1,265	72,494
Delta	87,381	8,714	96,095
Northwest	84,693	0	84,693
United	99,256	7,309	106,565
US Airways	94,188	1,036	95,224
Southwest	95,893	0	95,893
Total	**619,653**	**22,574**	**642,227**

Using the merged dataset, we then compute nominal times for ground turnaround and flight, ground and flight buffers, and propagated and newly formed delays for each flight node. The next subsection presents the computation results.

3.4 Results

3.4.1 Nominal times for ground turnaround and flight

We compute nominal turnaround time on ground links by airline and aircraft category (as the data is only for one quarter, seasonal variation is not relevant). Table 2 shows the average nominal ground turnaround times based on different percentile values. As expected, the nominal ground turnaround times for narrow body aircraft is significantly lower than for wide body aircraft. For Alaska, Northwest, and Southwest, no wide body operations are recorded. Among the narrow body fleets, the lowest nominal ground turnaround times are observed in Southwest, with 22 minutes at the 25th percentile. This is not surprising, as Southwest operates predominantly point-to-point services which do not require as much time as for a hub-and-spoke carrier for passenger connection at hub airports. The situation for wide body aircraft is more complicated. We observe that, when 50th and 75th percentile values are used, the calculated nominal ground turnaround time for Continental will be 108 and 277 minutes, which are very different from those of the other carriers. This may be because many Continental wide body aircraft do not fly much in a day and spend most time on the ground, resulting in inter-flight ground time much larger than nominal turnaround time. In contrast, the calculated nominal ground turnaround times are more consistent across airlines when 25th percentile values are considered. In view of this, we only use 25th percentile to compute nominal ground turnaround time in the rest of the paper.

Table 2: Nominal ground turnaround times

		Nominal ground turnaround time		
Carrier	Aircraft category	25th Percentile	50th Percentile	75th Percentile
American	NB	38	45	58
	WB	61	71	87
Alaska	NB	34	43	58
Continental	NB	42	52	70
	WB	62	108	277
Delta	NB	40	48	62
	WB	54	63	87
Northwest	NB	38	50	70
United	NB	37	45	59
	WB	61	80	119
US airways	NB	39	48	63
	WB	56	69	91
Southwest	NB	22	26	31

Note: NB: Narrow Body, WB: Wide Body

Figure 3 (a) presents the histogram of flights with respect to flight distance, for both narrow body (in brown) and wide body (in white) aircraft. It can be seen that narrow body aircraft cover more and generally shorter-haul flight segments than wide body aircraft. Figure 3 (b) gives boxplots of flight buffers at the 5th percentile and grouped by flight distance (<500 miles, 500-1000 miles, 1000-2000 miles, and > 2000 miles). The boxplots of flight buffers at the same percentile but grouped by local departure time in a day is displayed in Figure 3 (c). Overall, longer flights have greater buffers. However, the departure time effect

on flight buffer is less prevalent, although flight buffers tend to be more dispersed during busy hours (8:00 – 12:00 and 16:00 – 20:00). The same conclusions can be drawn when 10th and 20th percentile values are used.

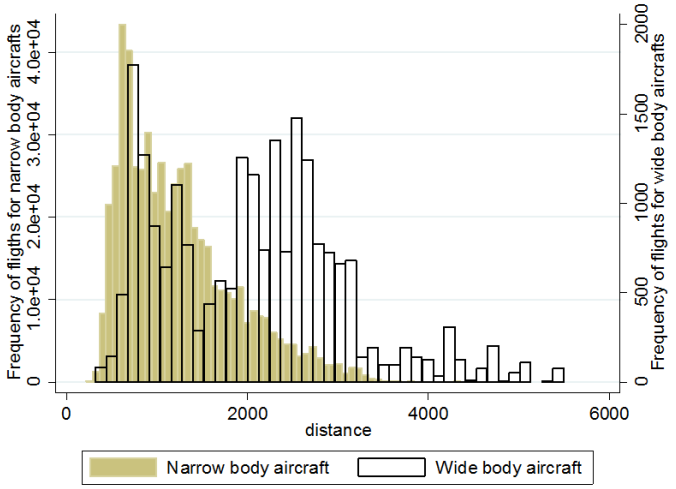

Figure 3 (a): Nominal flight operation times based on the 5th percentile actual flight times

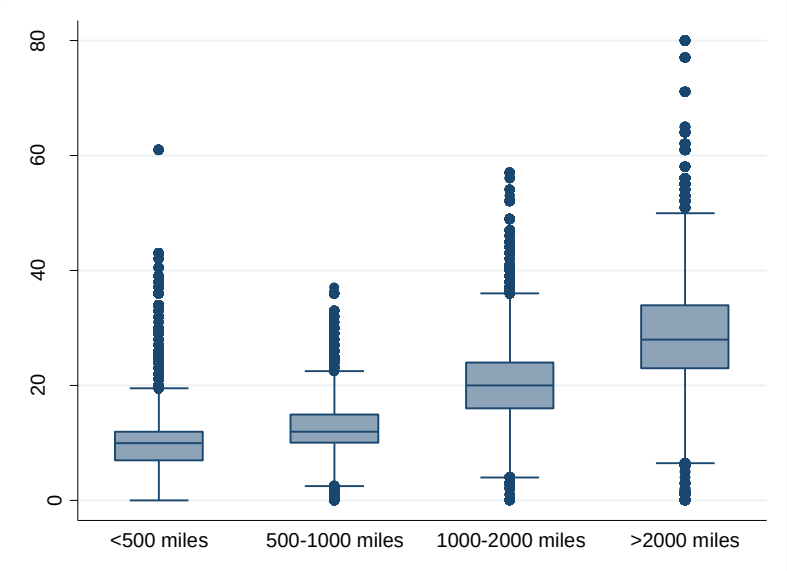

Figure 3 (b): Boxplots of flight buffers based on the 5th percentile actual flight times and grouped by flight distance (<500 miles, 500-1000 miles, 1000-2000 miles, and > 2000 miles)

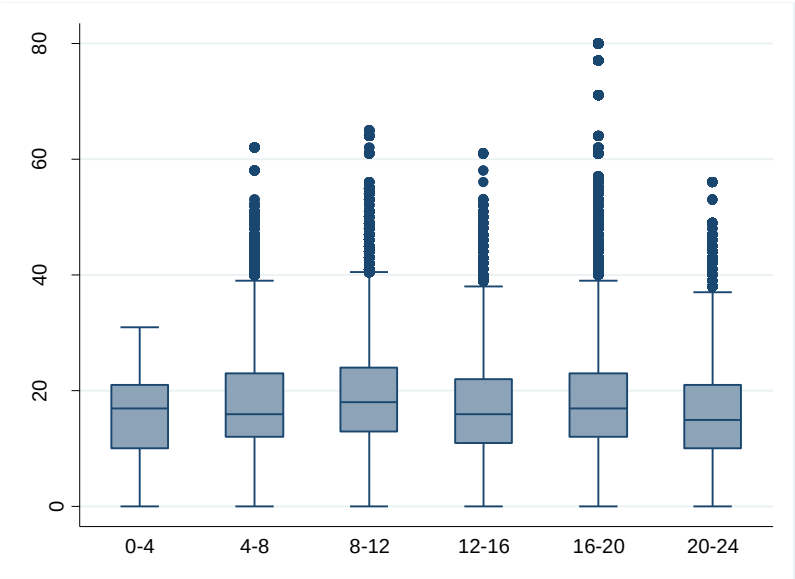

Figure 3 (c): Boxplots of flight buffers based on the 5th percentile actual flight times and grouped by local departure time in a day (0:00 – 4:00, 4:00 – 8:00, 8:00 – 12:00, 12:00 – 16:00, 16:00 – 20:00, 20:00 – 0:00)

3.4.2 Ground and flight buffers

Table 3 presents summary statistics for ground and flight buffers based on different percentile values from the actual times. The average ground buffer is around 23 minutes based on the 25th percentile actual turnaround time. The minimum value is 0 and the values are widely dispersed with standard deviation of 74 and a maximum value of 1015 minutes. Possible reasons for the wide dispersion may be due to scheduled aircraft maintenance between two flights, or simply that airlines do not schedule certain aircraft to fly much in a day (thus spending most time on the ground). In contrast to ground buffer, flight buffer is smaller and less dispersed. This implies greater heterogeneity associated with ground operations than flight operations.

Table 3: Summary statistics for ground and flight buffers (in minutes)

Variable	Mean	Std. Dev.	Min	Max
Ground buffer based on the 25th percentile actual time	23.30	73.46	0	1015
Flight buffer based on the 5th percentile actual time	18.05	8.32	0	80
Flight buffer based on the 10th percentile actual time	15.10	7.56	0	74
Flight buffer based on the 20th percentile actual time	9.80	6.30	0	63

3.4.3 Propagated delay

Table 4 shows summary statistics for total propagated delay (TPD) rooted in each node, with nominal times based on the 5th percentile actual flight time and the 25th percentile actual ground turnaround time (these percentile choices also apply to sections 3.4.4 and 3.4.5). Note that many nodes have zero newly formed delays, thus having no TPDs. In Table 4, only nodes with non-zero TPDs are considered in generating the summary statistics. TPDs for departure and arrival nodes are reported separately, as we speculate that departure and arrival nodes may exhibit different delay propagation patterns (this is further discussed in Section 4). The average TPD ranges from 19.48 to 44.96 minutes. We note that some propagated delays are too large, which may be caused by unexpected aircraft maintenance and measurement errors. To reduce the influence of such outliers, nodes with TPDs larger than the 75th percentile value plus 1.5 times the inter-quantile range are dropped from the dataset. Recall that by definition a node is associated

with a flight. Flights that are linked to the dropped flight by the same aircraft are also dropped. Depending on the scenarios, this excludes about 3-5% of flights from the original dataset. Summary statistics for the remaining data are shown in the lower half of Table 4.

Table 4: Summary statistics for total propagated delays (TPDs)

	Mean	Std. Dev.	Min	Max
Before dropping outlying values				
Scenario 1				
Total propagated delay from departure nodes	44.96	99.15	8e-16	2736.2
Total propagated delay from arrival nodes	26.83	49.46	3e-16	1776.49
Scenario 2				
Total propagated delay from departure nodes	43.30	93.40	2e-10	2693.25
Total propagated delay from arrival nodes	26.22	43.48	1e-09	1682.7
Scenario 3				
Total propagated delay from departure nodes	28.43	74.85	1e-15	2694.23
Total propagated delay from arrival nodes	19.48	36.62	1e-10	1630.5
After dropping outlying values				
Scenario 1				
Total propagated delay from departure nodes	19.08	23.49	8e-16	108.18
Total propagated delay from arrival nodes	14.63	16.27	3e-16	74.43
Scenario 2				
Total propagated delay from departure nodes	19.04	22.07	2e-10	99.16
Total propagated delay from arrival nodes	13.86	14.52	2e-09	69.16
Scenario 3				
Total propagated delay from departure nodes	8.84	11.74	1e-15	55.85
Total propagated delay from arrival nodes	8.58	10.42	1e-10	51.94

3.4.4 Temporal distribution of propagated and newly formed delays

In this subsection we present system total propagated and newly formed delays associated with the nodes aggregated by hour over all days in the dataset. The aggregation uses local time for each node. Again, departure and arrival nodes are considered separately. The first column in Figure 4 (i.e., (a), (c), (e)) represents newly formed delay at flight departure nodes (in dark blue) and total propagated delay from these nodes (in light blue). The second column in Figure 4 (i.e., (b), (d), (f)) shows newly formed delay at flight arrival nodes and total propagated delay from these nodes, using the same color notation. In each plot, x-axis denotes time and y-axis indicates total delay minutes. The first row (i.e., Figures 4(a) and 3(b)) corresponds to scenario 1; the second row scenario 2; and the third row scenario 3.

Overall, both newly formed and propagated delays are considerably lower from after midnight till early morning. This is the period in a day when most aircraft are grounded. Newly formed delay under scenario 1 is smaller than under scenarios 2 and 3, which is not surprising as in scenario 1 buffer first absorbs newly formed delay. In contrast, propagated delay under scenario 1 seems consistently larger than under the other two scenarios, which is especially true at flight departure nodes. Newly formed departure delays are generally greater than newly formed arrival delays, which suggest that departure delay is a more prominent phenomenon than arrival delay in the system.

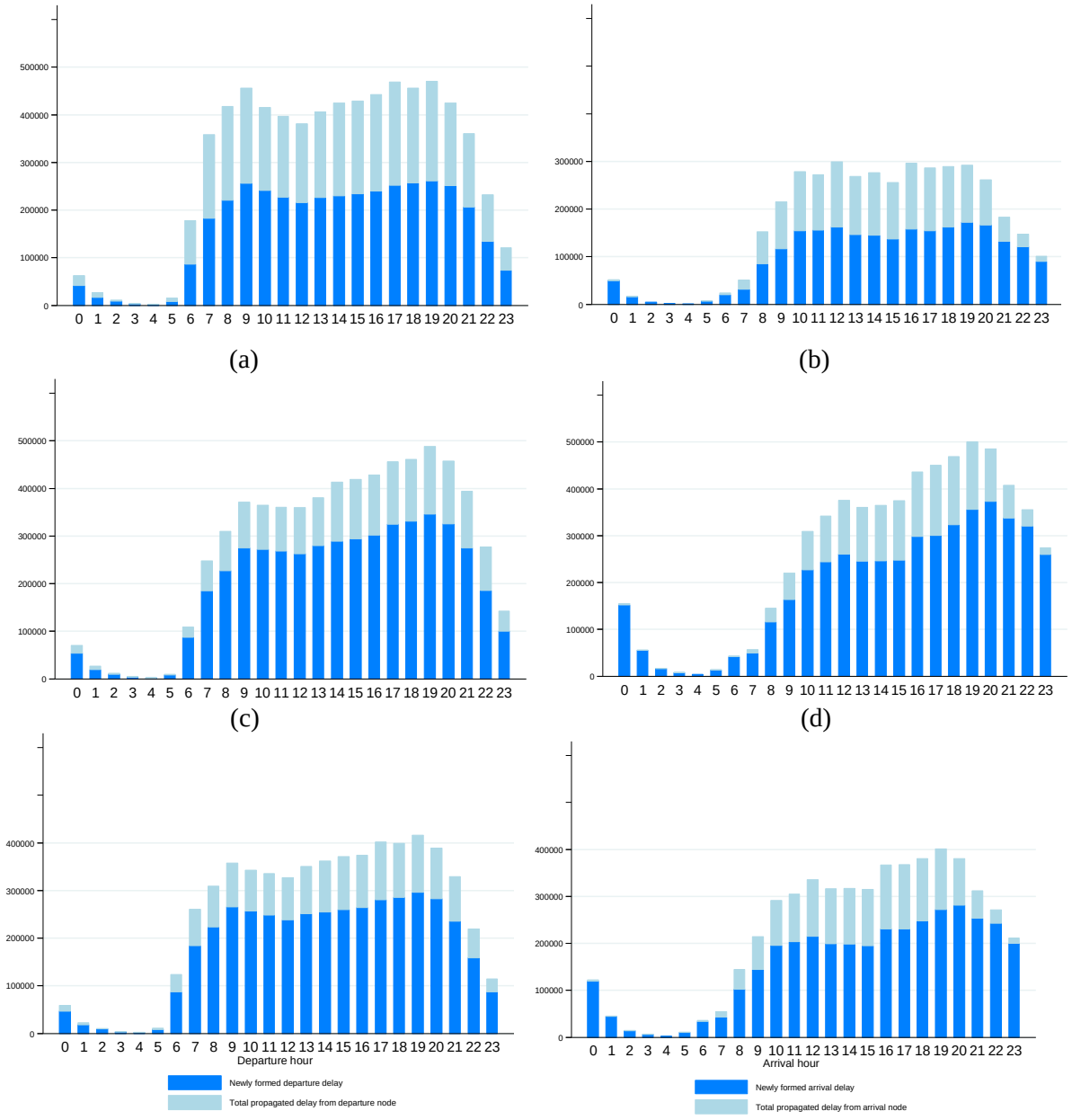

Figure 4: Temporal distribution of aggregated newly formed and total propagated delays at flight departure nodes under scenario 1 (a), scenario 2 (c), and scenario 3 (e); and at flight arrival nodes under scenario 1 (b), scenario 2 (d), and scenario 3 (f)

3.4.5 Spatial distribution of propagated and newly formed delays

The significance of newly formed and propagated delays varies by location as well as by time of a day. Figure 5 illustrates the amount of total newly formed departure delays (first column) and their propagated arrival delays (second column), by airport, in three time intervals: 7 - 8 am, 1 - 2 pm, and 10 - 11 pm in Eastern Standard Time (EST). The computation of newly formed and propagated delays is based on scenario 1 and uses all airports that appear in our dataset.

Overall, strong spatial and temporal heterogeneity exists in both types of delays. The distribution of the two types of delays are highly collinear, with a clear lag between the eastern and western parts of the

country. An exception is Chicago O'Hare International Airport, which experiences relatively high delays in all three periods. During 7 - 8 am EST, airports on the east coast already have considerable newly formed delays. These delays later generate comparable amounts of total propagated arrival delays. Delays during the same hour are in a less extent in the middle part of the country and even less so at western airports – in fact the local time on the west coast is 4 - 5 am and there is not so much traffic. During 1 - 2 pm, airports in the western region show increased delays, whereas the delay levels at eastern airports mostly experience some decrease. During 10 - 11 pm EST, the eastern airports approach the end of an operation day with minimum delays, whereas airports in the western part of the country are still in evening peaks and have more visible newly formed and consequently propagated delays.

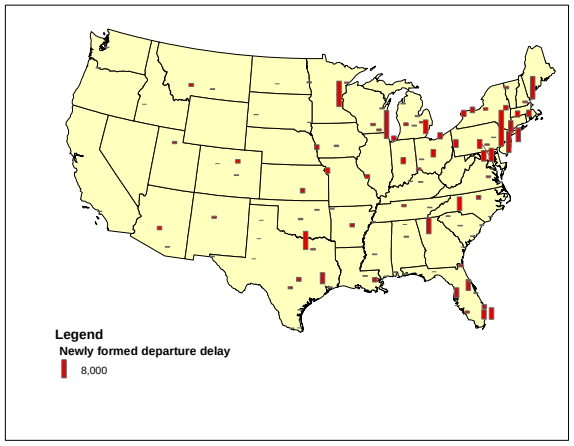

(a)

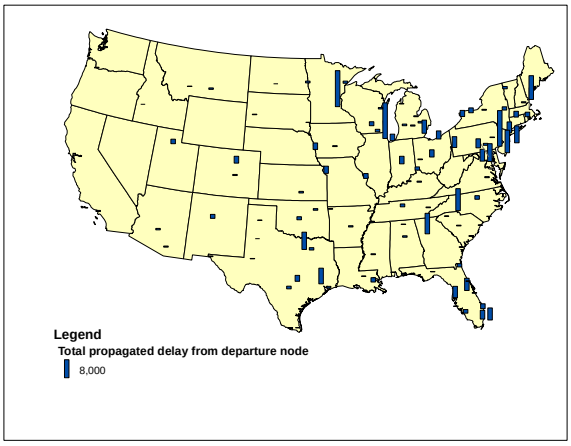

(d)

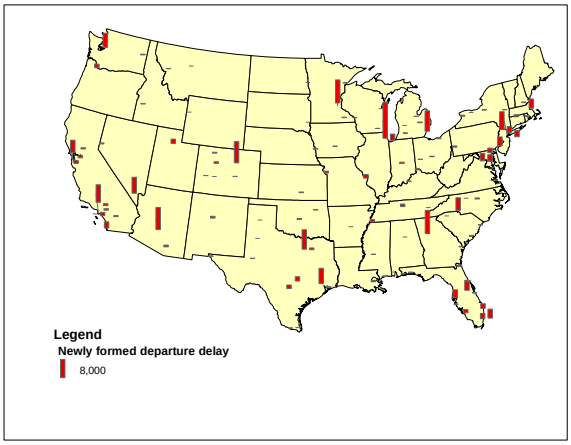

(b)

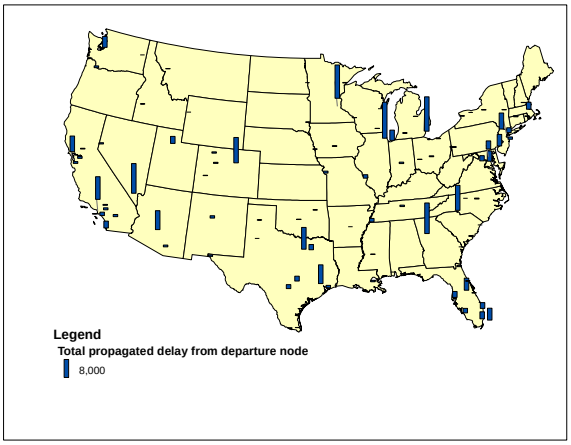

(e)

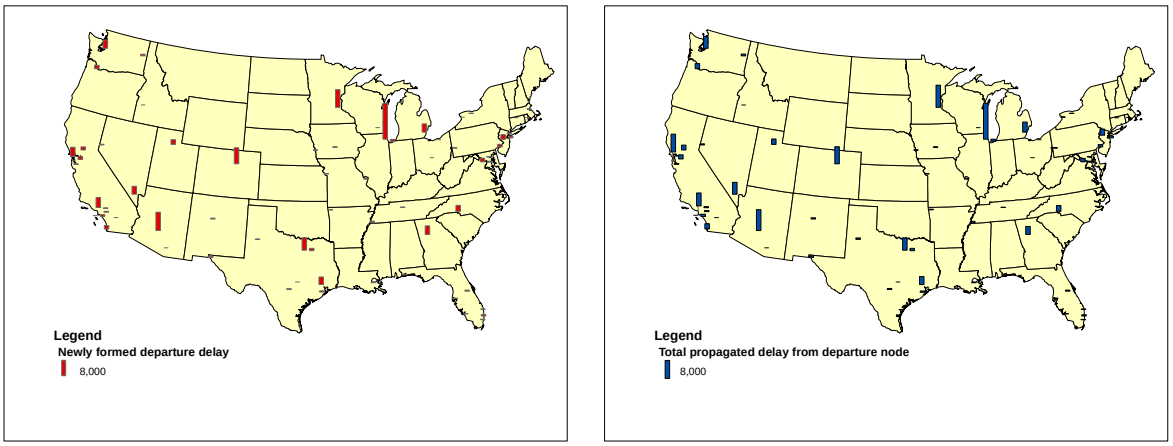

(c) (f)

Figure 5: Spatial-temporal distribution of newly formed departure delays (a-c) and their propagated delays (d-f), aggregated by state, during 7 - 8 am (a, d), 1 - 2 pm (b, e), and 10 - 11 pm (c, f), all in EST

4 Econometric modeling for the initiation and propagation of propagated delays

Besides computing propagated and newly formed delays, it remains unanswered under what conditions propagated delay is likely to appear, how the size of total propagated delay (TPD) is shaped as it goes downstream, and by what factors. To answer these questions, in this section we develop a novel econometric modeling framework that jointly quantifies the effect of various factors on the initiation and progression of propagated delay. We first provide a conceptual overview of the joint model below.

To answer the question of whether some newly formed delay at a node i (i.e., N_i) propagates, it suffices to look at its propagated delay to the immediate downstream node, i.e., $p_{i,i+1}$. This is because if $p_{i,i+1} > 0$, then delay propagation is initiated (otherwise, there will be no propagated delay). We hypothesize that the initiation of propagated delay depends on N_i and buffer on link $(i, i+1)$ (i.e., $B_{i,i+1}$)[3]. In addition, under scenarios 1 and 3 the initiation of propagated delay may be affected by newly formed delay at node $i+1$ (i.e., N_{i+1}), because N_{i+1} will be absorbed with at least the same priority as N_i under the two scenarios by available buffer. Under scenarios 2 and 3, N_i will further compete with propagated delay to node i (i.e., $\sum_{k=1}^{i-1} p_{k,i}$) for buffer.[4] The initiation problem can be modeled as a discrete, binary choice problem, with a 0-1 dependent variable indicating whether a node generates non-zero TPD.

When modeling the progression of TPD, we are only concerned with nodes that have positive delays. These nodes comprise a non-random sample in the original dataset. We hypothesize that the progression of propagated delay is shaped by four groups of factors: i) the severity of the newly formed delay (N_i); ii) propagated delay to node i ($\sum_{k=1}^{i-1} p_{k,i}$), which is absorbed together with N_i downstream of node i; iii) downstream mitigating factors including ground and flight buffers; and iv) the macro-congestion environment downstream. It should be noted that simply applying Ordinary Least Squares (OLS) to regress TPD_i on these factors would yield biased results due to non-random sample selection—the nodes selected to run regression are those which are more vulnerable to delay propagation than those unselected.

[3] When appropriate, $B_{i,i+1}$ needs to be updated by $B^a_{i,i+1}$ as discussed in Algorithms 2 and 3 in subsection 3.2.

[4] Under scenario 1, the competition between N_i and $\sum_{k=1}^{i-1} p_{k,i}$ for buffer would be secondary compared to the competition between N_i and N_{i+1}.

To prevent the potential bias brought by sample selection, we propose a joint discrete-continuous model that estimates initiation and progression of propagated delay simultaneously. A key in the joint model is that the error terms in the discrete delay initiation model and the continuous delay progression model are correlated. Below we detail the model specification.

4.1 Model specification

In our econometric model, the unit of observation is a departure or an arrival node defined in Section 2. For the initiation of propagated delay, we introduce a 0-1 indicator variable z_i for each node i and an associated latent variable z_i^* whose value is a linear combination of independent variables $\boldsymbol{w}_i$ (with $\boldsymbol{\gamma}$ being the combination coefficients) and a random error term u_i:

$$z_i^* = \boldsymbol{w}_i\boldsymbol{\gamma} + u_i \tag{11}$$

where as mentioned above two common variables in $\boldsymbol{w}_i$ across all three scenarios are N_i and $B_{i,i+1}$. Under scenarios 1 and 3, N_{i+1} is further included in $\boldsymbol{w}_i$; so is $\sum_{k=1}^{i-1} p_{k,i}$ under scenarios 2 and 3.

Scenario 1: N_i, $B_{i,i+1}$, N_{i+1};

Scenario 2: N_i, $B_{i,i+1}$, $\sum_{k=1}^{i-1} p_{k,i}$;

Scenario 3: N_i, $B_{i,i+1}$, $\sum_{k=1}^{i-1} p_{k,i}$, N_{i+1};

The relationship between z_i and the latent variable z_i^* is that

$$z_i = 1 \text{ if } z_i^* > 0;\ z_i = 0 \text{ if } z_i^* < 0 \tag{12}$$

Assuming that u_i follows a standard normal distribution, we model the sample selection (i.e., selecting nodes that have non-zero TPDs) using a Probit specification:

$$\text{Prob}(z_i = 1|\boldsymbol{w}_i) = \Phi(\boldsymbol{w}_i\boldsymbol{\gamma});\ \text{Prob}(z_i = 0|\boldsymbol{w}_i) = 1 - \Phi(\boldsymbol{w}_i\boldsymbol{\gamma}) \tag{13}$$

where $\Phi(\cdot)$ is the cumulative distribution function of the standard normal distribution.

The progression of delay propagation is modeled as a linear combination of independent variables $\boldsymbol{x}_i$ (with $\boldsymbol{\beta}$ being the combination coefficients) and a random error term ε_i:

$$y_i = \boldsymbol{x}_i\boldsymbol{\beta} + \varepsilon_i \text{ observed only if } z_i = 1 \tag{14}$$

where y_i is the total propagated delay from node i (TPD_i). We consider two types of TPD_i based on whether i is a departure node (thus propagated delay from a newly formed departure delay) or an arrival node (thus propagated delay from a newly formed arrival delay). The hypothesis is that departure and arrival nodes may have different delay propagation patterns.

For the independent variables $\boldsymbol{x}_i$, three groups of variables are included: delays at node i, ground and flight buffers on downstream links, and the macro-congestion environment downstream. The first group contains two variables: N_i and $\sum_{k=1}^{i-1} p_{k,i}$. For N_i, we hypothesize that the severity of the newly formed delay positively correlates with the amount of delay it can propagate. Knowing $TPD_i > 0$, newly formed delay at node i (N_i) will compete with propagated delay to node i ($\sum_{k=1}^{i-1} p_{k,i}$) for being absorbed by buffer as both propagate downstream. Thus these two variables both affect the size of TPD_i.

The second group of variables, ground and flight buffers on downstream links, plays the role of reducing propagated delays. Recall that flight operations considered in this study are between 6 am and 10 pm. For the aircraft that is associated with the node of concern, we group and sum ground and flight buffers on downstream links of the node to each of the four time groups: 6 am – 10 am, 10 am – 2 pm, 2 pm – 6 pm, and 6 pm – 10 pm (buffers prior to the node of concern are given value zero). The grouping of downstream ground buffers is based on the local time of the departure node on the corresponding ground link. Similar

grouping and summation are performed on flight buffers, except that the grouping of flight buffers is based on the local time of the arrival node on a corresponding flight link.

The third group of variables, which reflects the macro-congestion environment downstream, controls for the propensity of forming new delays downstream of node i, which affects the extent to which N_i further propagates or is absorbed. We introduce average airport arrival delay during each hour between 6 am and 10 pm local time (thus in total 16 such variables are constructed). The average airport arrival delay for a given hour is calculated by dividing the total flight delay minutes by the total number of flights that actually arrived at an airport in that hour (measured in local time). The airport-hour correspondence is identified by the downstream arrival nodes. Let us refer back to Figure 1 to illustrate this. If one is interested in total propagation delay from the departure node (DEN, 10:10 am), then the average airport hourly arrival delays included would be at (DFW, 1-2 pm), (PHX, 3-4 pm), and (LAS, 4-5 pm), all in local time. For hours that do not have a downstream arrival node, the average airport arrival delays take value zero.

We assume that ε_i follows a normal distribution: $\varepsilon_i \sim N(0, \sigma_\varepsilon^2)$. In addition, the error terms u_i and ε_i are correlated with correlation coefficient ρ. The intuition is that the sample of nodes with non-zero propagated delays would be nodes that are more vulnerable to delay propagation. The error terms are is specified to have a joint normal structure:

$$(u_i, \varepsilon_i) \sim N[\begin{pmatrix}0\\0\end{pmatrix}, \begin{pmatrix}1 & \rho\\ \rho & \sigma_\varepsilon^2\end{pmatrix}] \tag{15}$$

Using the results on multivariate distributions (Johnson and Kotz, 1974; Greene, 2012), the expected value for y_i conditional on $z_i = 1$ is

$$\begin{aligned} E(y_i|z_i = 1) &= E(y_i|z_i^* > 0) = E(y_i|u_i > -\boldsymbol{w}_i\boldsymbol{\gamma}) = \boldsymbol{x}_i\boldsymbol{\beta} + E(\varepsilon_i|u_i > -\boldsymbol{w}_i\boldsymbol{\gamma}) \\ &= \boldsymbol{x}_i\boldsymbol{\beta} + \rho\sigma_\varepsilon \frac{\phi(\boldsymbol{w}_i\boldsymbol{\gamma})}{\Phi(\boldsymbol{w}_i\boldsymbol{\gamma})} = \boldsymbol{x}_i\boldsymbol{\beta} + \beta_\lambda \frac{\phi(\boldsymbol{w}_i\boldsymbol{\gamma})}{\Phi(\boldsymbol{w}_i\boldsymbol{\gamma})} \end{aligned} \tag{16}$$

where $\beta_\lambda = \rho\sigma_\varepsilon$ and $\phi(\cdot)$ is the probability density function (PDF) of the standard normal distribution. Thus

$$y_i|z_i^* > 0 = E(y_i|z_i = 1) + \varepsilon_i = \boldsymbol{x}_i\boldsymbol{\beta} + \beta_\lambda \frac{\phi(\boldsymbol{w}_i\boldsymbol{\gamma})}{\Phi(\boldsymbol{w}_i\boldsymbol{\gamma})} + \varepsilon_i \tag{17}$$

It is now clear that OLS regression of $y_i|z_i^* > 0$ on $\boldsymbol{x}_i$ would produce inconsistent estimates for $\boldsymbol{\beta}$ due to omitting variable $\frac{\phi(\boldsymbol{w}_i\boldsymbol{\gamma})}{\Phi(\boldsymbol{w}_i\boldsymbol{\gamma})}$.

4.2 Estimation method

Two possible methods may be used to estimate the coefficients in the econometric model for the initiation and progression of propagated delays. One is Heckman's two-step procedure (Heckman, 1979), which estimates the initiation and progression parts of the model sequentially. The other, full information maximum likelihood (FIML) method, estimates both parts simultaneously. We have experimented with both methods, which yield consistent results. To keep the length of the paper we only report results from the Heckman's two-step procedure, which is also computationally easier.

Under the Heckman's two-step procedure, the initiation of propagated delays is estimated first. The results are then used in the second step to estimate the progression part. Specifically:

Step 1: Estimate Probit model (13) by maximum likelihood to obtain estimated coefficients $\widehat{\boldsymbol{\gamma}}$. For each observation with non-zero propagated delay, compute $\frac{\phi(\boldsymbol{w}_i\widehat{\boldsymbol{\gamma}})}{\Phi(\boldsymbol{w}_i\widehat{\boldsymbol{\gamma}})}$,

Step 2: Estimate the linear regression model (17) by OLS on the sample with non-zero propagated delays. This gives estimates $\widehat{\boldsymbol{\beta}}$ and $\hat{\beta}_\lambda$.

The caveat here is that the covariance matrix for $[\widehat{\boldsymbol{\beta}}\ \hat{\beta}_\lambda]$ differs from the traditional one under OLS. This is because the error term $\varepsilon_i|z_i = 1, \boldsymbol{w}_i, \boldsymbol{x}_i$ is heteroskedastic (Heckman, 1979; Greene, 2012): $\text{var}(\varepsilon_i|z_i = 1, \boldsymbol{w}_i, \boldsymbol{x}_i) = \sigma_\varepsilon^2(1 - \rho^2\delta_i)$, where $\delta_i = \frac{\phi(\boldsymbol{w}_i\boldsymbol{\gamma})}{\Phi(\boldsymbol{w}_i\boldsymbol{\gamma})}\left(\frac{\phi(\boldsymbol{w}_i\boldsymbol{\gamma})}{\Phi(\boldsymbol{w}_i\boldsymbol{\gamma})} + \boldsymbol{w}_i\boldsymbol{\gamma}\right)$. Using the estimated $\hat{\delta}_i = \frac{\phi(\boldsymbol{w}_i\widehat{\boldsymbol{\gamma}})}{\Phi(\boldsymbol{w}_i\widehat{\boldsymbol{\gamma}})}\left(\frac{\phi(\boldsymbol{w}_i\widehat{\boldsymbol{\gamma}})}{\Phi(\boldsymbol{w}_i\widehat{\boldsymbol{\gamma}})} + \boldsymbol{w}_i\widehat{\boldsymbol{\gamma}}\right)$, $\hat{\beta}_\lambda$, and residuals $\hat{\varepsilon}_i$, a consistent estimator of σ_ε^2 can be obtained as

$$\hat{\sigma}_\varepsilon^2 = \frac{\hat{\varepsilon}_i'\hat{\varepsilon}_i + \hat{\beta}_\lambda^2\sum_{j=1}^{N}\hat{\delta}_j}{N} \tag{18}$$

where N is the number of observations used in Step 2 regression. The consequent estimator for the correlation coefficient ρ is

$$\hat{\rho} = \frac{\hat{\beta}_\lambda}{\hat{\sigma}_\varepsilon} \tag{19}$$

Due to Greene (1981), the variance-covariance matrix for $[\widehat{\boldsymbol{\beta}}\ \hat{\beta}_\lambda]$ is

$$\text{Var}[\widehat{\boldsymbol{\beta}}\ \hat{\beta}_\lambda] = \hat{\sigma}_\varepsilon^2[\mathbf{X}_*'\mathbf{X}_*]^{-1}[\mathbf{X}_*'(\mathbf{I} - \hat{\rho}^2\hat{\Delta})\mathbf{X}_* + \mathbf{Q}][\mathbf{X}_*'\mathbf{X}_*]^{-1} \tag{20}$$

where $\mathbf{X}_* = \left[\left[\boldsymbol{x}_1\ \frac{\phi(\boldsymbol{w}_1\widehat{\boldsymbol{\gamma}})}{\Phi(\boldsymbol{w}_1\widehat{\boldsymbol{\gamma}})}\right]; \ldots; \left[\boldsymbol{x}_i\ \frac{\phi(\boldsymbol{w}_i\widehat{\boldsymbol{\gamma}})}{\Phi(\boldsymbol{w}_i\widehat{\boldsymbol{\gamma}})}\right]; \ldots; \left[\boldsymbol{x}_N\ \frac{\phi(\boldsymbol{w}_N\widehat{\boldsymbol{\gamma}})}{\Phi(\boldsymbol{w}_N\widehat{\boldsymbol{\gamma}})}\right]\right]$; $\mathbf{I} - \hat{\rho}^2\hat{\Delta}$ is a diagonal matrix of dimension $N \times N$ with $(1 - \hat{\rho}^2\hat{\delta}_i)$ being the ith $(i = 1, \ldots, N)$ diagonal element; $\mathbf{Q} = \hat{\rho}^2\left[\mathbf{X}_*'\hat{\Delta}\mathbf{W}\right]\text{Var}[\widehat{\boldsymbol{\gamma}}][\mathbf{W}'\hat{\Delta}\mathbf{X}_*]$ in which $\mathbf{W} = [\boldsymbol{w}_1; \ldots; \boldsymbol{w}_i; \ldots; \boldsymbol{w}_N]$ and $\text{Var}[\widehat{\boldsymbol{\gamma}}]$ is the variance-covariance matrix for $\widehat{\boldsymbol{\gamma}}$ obtained from Step 1.

4.3 Estimation results

As mentioned in subsection 4.1, separate models for TPD_i with i being a departure node and an arrival node are estimated. In conjunction with the three scenarios for delay absorption, in total six models are estimated for given percentile values that determine flight and ground buffers. In the interest of space, detailed estimation results of the models using 5th percentile value for flight buffer and 25th percentile value for ground buffer computation are presented in Appendix C. Later in this subsection, we also report the sensitivity of model estimates using other percentile values for flight buffer.

Across all six models, most of the coefficients are significant and have expected signs. For the initiation of propagated delay, the coefficients of newly formed departure (arrival) delay at the current node i is positive, confirming a positive correlation between newly formed delay and the likelihood of delay propagation. The magnitude of influence is about 3-4 times larger at a departure node than at an arrival node. The negative coefficient for $B_{i,i+1}$ is expected: greater buffer reduces the chance of propagated delay being initiated. The buffer effect is smaller than the effect of newly formed delay, which is especially true when the nodes chosen correspond to arrivals.

Under scenarios 1 and 3 where propagated delay has at most equal priority with newly formed delay for being absorbed by buffer, the extent that N_i will be absorbed depends on the amount of N_{i+1}. The higher N_{i+1}, the greater chance that N_i will propagate to node $i + 1$. This conjecture is corroborated by the positive coefficient for N_{i+1}. However, the effect of N_{i+1} is considerably lower than the effect of N_i. Under scenarios 2 and 3, the coefficients for $\sum_{k=1}^{i-1} p_{k,i}$ are also positive, as expected. Because $\sum_{k=1}^{i-1} p_{k,i}$ competes with N_i for buffer, the higher the $\sum_{k=1}^{i-1} p_{k,i}$, the greater chance that N_i will propagate to node $i + 1$. Similar to the N_{i+1} variable, the effect of $\sum_{k=1}^{i-1} p_{k,i}$ is smaller than the effect of N_i.

Turning to the progression part for propagated delay, the estimates show that N_i significantly affects the size of TPD_i. Again, the positive effect is larger at departure nodes than at arrival nodes (note that there is a negative coefficient for arrival nodes under scenario 2). $\sum_{k=1}^{i-1} p_{k,i}$ has a positive coefficient across all progression models (except for delay at arrival nodes under scenario 2), which can be explained as follows: now that N_i is known to progress downstream, it competes with $\sum_{k=1}^{i-1} p_{k,i}$ for absorption given an amount of buffer.

The ground and flight buffer variables generally have the expected negative signs, with the exception under scenario 1, where significant positive coefficients are obtained for departure nodes. The counter-intuitive sign may imply that scenario 1 be a less likely characterization of the way delays are absorbed by buffer. The general trend for the ground buffer coefficients is that the delay mitigation effect is greater at earlier time periods than later. As an example, ground buffer in time group 1 is 2.9 (-0.047/(-0.016)) times more effective than in time group 4 for the model in the last column in Table C.3. Such a trend seems less prominent for flight buffers.

Finally, the coefficients for the average airport arrival delays in each hour are mostly positive, which supports our hypothesis that a more congested macro-environment downstream aggravates delay propagation. The effects do not strictly increase over the course of hours, but follows a more general first-increase-then-decrease trend, which is in accord with conventional wisdom: on the one hand, as it is getting into the middle of a day, air traffic and consequently congestion grow, making propagated delay more vulnerable to further progression; on the other hand, as the day is approaching its end, air traffic congestion dwindles. As a result the impact of macro-congestion environment on delay propagation diminishes.

Recall that the results presented here are based on the 5^{th} percentile value for flight buffer and 25^{th} percentile value for ground buffer computation. To test the sensitivity of the results to difference percentile choices, we also estimate the models with other buffer values. For the interest of space, here we only present in Table 5 the coefficient estimates for newly formed departure and arrival delays in the progression part of the models with different flight buffers. As buffer is the difference between the scheduled time and a chosen percentile time (given in parenthesis in table 5), a greater percentile value means a smaller buffer value. We observe that both coefficients for newly formed departure and arrival delays decrease with the increase in buffer values, with greater sensitivity occurring to arrival delay. The explanation for the decreasing trend is intuitive: if one believes that there is less buffer in the schedule, then the effects of newly formed delays on delay propagation would be perceived greater.

Table 5: Sensitivity of newly formed departure and arrival delay coefficients in the progression part of the model with different values for flight buffer

Average calculated flight buffer	Coefficient of newly formed delay	
	Departure node	Arrival node
18.05 mins (5^{th} percentile)	0.767	0.463
15.1 mins (10^{th} percentile)	0.785	0.498
9.8 mins (20^{th} percentile)	0.801	0.551

4.4 Implication for airport- and airline-specific delay propagation

This subsection extends the previously estimated model by looking into airport- and airline-specific progression of propagate delays. The results presented here are based on scenario 3, although the general insights are consistent if considering the other two scenarios.

For airport-specific delay propagation, we re-estimate the model for 10 airports that had the most flight arrivals in the dataset. More specifically, given an airport, only observations whose departure (or arrival) node corresponds to the airport chosen are used for model estimation. Figure 6 (a) reports the estimated coefficients for newly formed departure and arrival delays. We find that six out of the 10 airports have larger coefficients than the system average for newly formed departure delay, and five airports have larger coefficients for newly formed arrival delay. The estimated coefficients for newly formed delays are important to airport authorities as it can also be interpreted as the average reduction in propagated delay as a result of newly formed delay reduction. Take DTW for example. If the newly formed arrival delay for all flights using the airport were reduced by 1 minutes due to airport capacity expansion, then the propagated delay of these flights would be 0.903 minutes less. Comparison of these airport-specific coefficients for newly formed delays may help aviation system planners such as the FAA gain deeper insights into flight

delay propagation patterns and consequently prioritize resource allocation while improving system overall performance.

We similarly estimate airline-specific models for each of the eight airlines in our dataset. Figure 6 (b) plots the estimated coefficients for both newly formed departure and arrival delays. Southwest has the largest coefficient for both newly formed departure and arrival delays, which is consistent with the fact that the airline has the lowest buffer (see Table 2). As Southwest operates a predominately point-to-point service model, the results also suggest a negative relationship between the delay propagation multiplier and the extent of point-to-point service structure adopted.[5] Among the remaining network carriers, the coefficients for newly formed departure delay are fairly close. The same is true for the coefficients for newly formed arrival delay with the exception of American. These airline-specific coefficients, together with other coefficient estimates for the initiation and progression of propagated delay, can be useful to airlines in assigning buffer to flight schedules and controlling airline-wide operational performance to mitigate delay propagation.

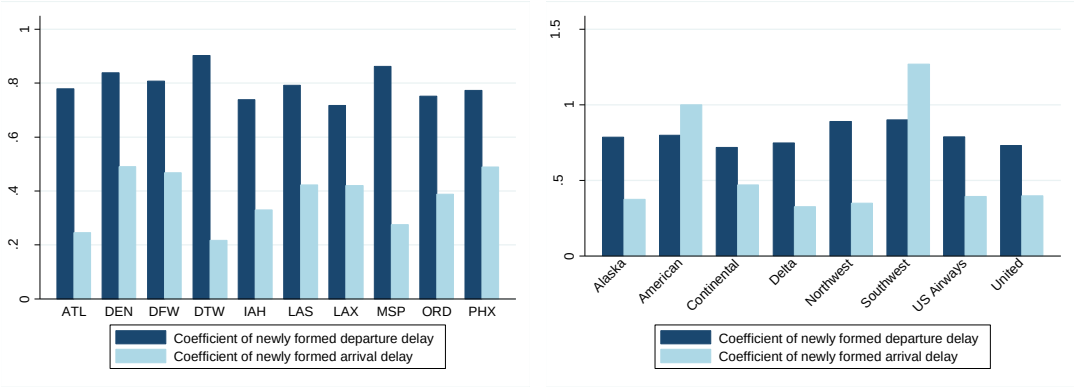

(a) (b)

Figure 6: Delay propagation multiplier for different (a) airports and (b) airlines

Finally, we compare the estimated delay propagation multipliers with the ones from the literature. More specifically, delay propagation multipliers were reported or can be inferred from three studies (Beatty et al., 1998; Welman et al., 2010; Churchill et al., 2010). To make consistent comparison, our multiplier needs to be augmented by 1, as those reported in the literature include initial delay in the multiplier computation. By and large, our results are in line with the existing findings in spite of different methodologies used. For example, Beatty et al. (1998) obtained delay multipliers which are differentiated by flight departure time and the amount of initial delay, spanning a wide range from 1.1 to 7.6. The authors did not account for the role of buffer in delay reduction. The delay propagation multipliers in Welman et al. (2010) are close to our estimates with two differences: 1) only propagated arrival delays were counted; 2) buffers were not considered. These two differences tend to deviate their estimates from ours in opposite directions, thus likely to cancel out to a large extent. Churchill et al. (2010) recognized the presence of ground buffer and found that propagated delays constitute 20%-30% of total flight delays, among flights with and without propagated delays. This is different from the progression part of our model where only flights with propagated delays are considered. Nonetheless, their estimates translate to multiplier values between 1.25 (1+0.2/(1-0.2)) and 1.43 (1+0.3/(1-0.3)), which are again consistent with our estimates.

[5] While constructing a metric to precisely measure the extent to which an airline uses point-to-point vs. hub-and-spoke services is beyond the scope of the present paper, previous empirical research did reveal that the extent of hubbing by Southwest is substantially lower than the other airlines considered here. For example, Baumgarten et al. (2014) obtained the average Hubbing Concentration Index value of Southwest to be 87 between 2003 and 2010. During the same period the index values for United, American, and Delta were all above 250. Similar significant gaps were confirmed in Martin and Voltes-Dorta (2009). We thank one of the anonymous reviewers for raising this point.

5 Conclusion

A flight may be late arriving at or departing from an airport due to delays that occurred much earlier in the day. A small amount of initial flight delay can propagate downstream and compromise the on-time performance of the overall operations of the same aircraft. Ground and flight buffers are introduced so as to absorb both newly formed and propagated delays. To understand the delay propagation pattern and in particular the role played by different buffers in mitigating delay propagation, this study makes two methodological contributions: first, an analytical model is developed providing three different perspectives to quantify how flight delay propagates from any upstream node to any downstream node of the same aircraft. This analytical approach is applied to the US air transportation system using publically available data. Second, we develop a joint discrete-continuous econometric model and use Heckman's two-step procedure to reveal the effects of various influencing factors on the initiation and progression of propagated flight delays. The results are generally robust to the different scenarios that delays are absorbed by buffers and to the buffer values chosen. Estimation of the joint econometric model allows us to gauge the importance of newly formed delay to delay propagation specific to individual airports and airlines.

The analytical and empirical models developed in this study may help decision making by aviation system planners and airlines. With airport-specific insights into delay propagation, aviation system planners could be better informed about where to increase capacity while making infrastructure investment decisions. Airlines could potentially use the analytical model to analyze their flight scheduling practice, and identify and improve critical flights and ground operations, where inserting additional buffer will be most beneficial. Given the still dearth of knowledge on flight delay propagation vis-à-vis its pervasiveness in the air transportation system, the ability to understand and mitigate propagated flight delays is of great relevance. Our study contributes to enhancing this ability.

The present approaches can be further extended in a few directions. Among them, we think the following three are of special interest. First, this study focuses on delay propagation within each aircraft. Delay propagation from one aircraft to a second aircraft, which occurs due to passenger and crew connections and due to connected airport resources, is not explicitly accounted for. In effect, in our paper such propagated delay is considered as newly formed delay for the latter aircraft. The difficulty is that existing data do not provide direct information to distinguish between this type of propagated delay and the newly formed delay that is truly caused by an aircraft itself. It would be interesting to investigate potential ways to make the distinction. Second, our dataset contains observations (although a very small portion) with extended periods of ground turnaround due to aircraft maintenance and mechanical checks, the latter required by the FAA. Such activities may be scheduled or may occur unexpectedly. When scheduled, such operations affect our analysis by giving a large buffer time for ground turnaround (as seen in Table 3). On the other hand, if very long ground turnarounds occur unexpectedly, they result in large newly formed ground delays. This large newly formed ground delay, in turn, results in very large amount of total propagated delay (as seen in Table 4). These errors, if not controlled, could compromise the econometric model results. Future research may look into ways to identify such activities and assign different nominal turnaround times. Third, the finding that departure and arrival nodes have different delay propagation patterns may depend on the way we compute total propagated delay from a node, and nominal flight and ground turnaround times. Further investigation may be warranted to test whether this finding holds with alternative ways to construct these time variables. Overall, we hope that our effort will stimulate further investigations along this line of research towards deeper knowledge on the phenomenon of flight delay propagation and means to mitigate it.

Acknowledgement

We would like to thank Professor Mark Hansen and the two anonymous reviewers whose constructive comments have helped us substantially improve the quality of the paper.

Appendix A: Deriving propagated and newly formed delays under Scenario 1

Case 1 (a): $O_i > O_{i-1}$

In this case, the propagated delay from upstream nodes to node i, P_i, would not be absorbed at all and be equal to the observed delay at node $i-1$, O_{i-1}:

$$P_i = O_{i-1} \tag{A.1}$$

Newly formed delay at node i, N_i, after using flight buffer $B_{i-1,i}$, is the difference between observed delay and propagated delay at the node:

$$N_i = O_i - P_i = O_i - O_{i-1} \tag{A.2}$$

The propagated delay P_i can be disentangled by root. In principle, the roots can be all upstream nodes from the first node to node $i-1$. Letting $p_{k,i}$ denote the amount of propagated delay to node i whose root is in upstream node $k = 1,..i-1$, P_i can be rewritten as

$$P_i = \sum_{k=1}^{i-1} p_{k,i} \tag{A.3}$$

Given $O_i > O_{i-1}$, propagated delay from upstream nodes is not absorbed at all between nodes $i-1$ and i. Therefore we have

$$\sum_{k=1}^{i-1} p_{k,i} = O_{i-1} = \sum_{k=1}^{i-2} p_{k,i-1} + N_{i-1} \tag{A.4}$$

where $p_{k,i-1} = p_{k,i}$ for $k = 1,..,i-2$. Consequently

$$p_{i-1,i} = N_{i-1} \tag{A.5}$$

which says that the propagated delay whose root is the immediate upstream node is simply the newly formed delay at the immediate upstream node.

Case 1 (b): $O_i \leq O_{i-1}$

In this case, flight buffer absorbs all newly formed delays that occur during the flight from node $i-1$ to node i. No newly formed delay is present at node i. In addition, an amount of $O_{i-1} - O_i$ propagated delay will be reduced, leaving only O_i as the propagated delay at node i. Mathematically,

$$N_i = 0 \tag{A.6}$$

$$P_i = O_i - N_i = O_i \tag{A.7}$$

Similar to case 1 (a), $P_i = \sum_{k=1}^{i-1} p_{k,i}$. To calculate each $p_{k,i}$, we assume that the propagated delays with different roots are absorbed while maintaining their proportions. Thus root-specific propagated delays at node i are obtained by

$$p_{i-1,i} = N_{i-1} * \frac{O_i}{O_{i-1}} \tag{A.8}$$

$$p_{k,i} = p_{k,i-1} * \frac{O_i}{O_{i-1}} \quad \forall k = 1,...i-2 \tag{A.9}$$

Appendix B: Deriving propagated and newly formed delays under Scenario 2

Case 2 (a): $O_i > O_{i-1}$ and $B_{i-1,i} < O_{i-1}$

In this case, buffer on link $(i-1, i)$ is smaller than the observed delay at node $i-1$. All the buffer is used to absorb the propagated delay from all upstream nodes to node i. After absorption, an amount of propagated delay equal to $O_{i-1} - B_{i-1,i}$ remains at node i:

$$P_i = O_{i-1} - B_{i-1,i} \tag{A.10}$$

which is equivalent to

$$P_i = O_{i-1}[1 - \frac{B_{i-1,i}}{O_{i-1}}] \tag{A.11}$$

Substituting P_i and O_{i-1} by $\sum_{k=1}^{i-1} p_{k,i}$ and $N_{i-1} + \sum_{k=1}^{i-2} p_{k,i-1}$, we obtain

$$\sum_{k=1}^{i-1} p_{k,i} = (N_{i-1} + \sum_{k=1}^{i-2} p_{k,i-1}) * [1 - \frac{B_{i-1,i}}{O_{i-1}}] \tag{A.12}$$

Noting that propagated delays rooted in all upstream nodes are absorbed proportionally, we have

$$p_{i-1,i} = N_{i-1}[1 - \frac{B_{i-1,i}}{O_{i-1}}] \tag{A.13}$$

$$p_{k,i} = p_{k,i-1}[1 - \frac{B_{i-1,i}}{O_{i-1}}] \quad \forall k = 1, \dots i-2 \tag{A.14}$$

Because $O_i > O_{i-1}$, the observed delay at node i also contains some newly formed delay, which is

$$N_i = O_i - P_i = O_i - O_{i-1}[1 - \frac{B_{i-1,i}}{O_{i-1}}] \tag{A.15}$$

Case 2 (b): $O_i > O_{i-1}$ and $B_{i-1,i} > O_{i-1}$

In this case, buffer not only fully absorbs all propagated delay from upstream nodes to node i (which is equal to observed delay at node $i-1$), but also reduces part of the newly formed delay. All delays in O_i are newly formed on link $(i-1, i)$. Thus

$$P_i = 0 \tag{A.16}$$

$$N_i = O_i - P_i = O_i \tag{A.17}$$

Case 2(c): $O_i < O_{i-1}$ and $B_{i-1,i} < O_{i-1}$

In this case, buffer is entirely used to absorb propagated delay. Still, as $B_{i-1,i} < O_{i-1}$, some propagated delay equal to $O_{i-1} - B_{i-1,i}$ remains at node i. Newly formed delay at node i is the difference between the observed delay and the propagated delay, i.e., $N_i = O_i - P_i = O_i - \left(O_{i-1} - B_{i-1,i}\right) = O_i + B_{i-1,i} - O_{i-1}$.

There is a caveat here. It is possible that $O_i + B_{i-1,i} < O_{i-1}$. This occurs when buffer for this particular flight is actually larger than the calculated value $B_{i-1,i}$. Recall that we consider $5^{th}/10^{th}/20^{th}$ percentile values of observed flight times as the nominal flight operation times. As a result, 5%/10%/20% of total flights would fly shorter than the nominal flight operation time. For these flights, our approach is to adjust their buffer values to $O_i - O_{i-1}$. By doing so, we implicitly assume that zero new delay is formed. A unified expression encompassing this special circumstance is as follows:

$$B^a_{i-1,i} = \max(B_{i-1,i}, O_{i-1} - O_i) \tag{A.18}$$

$$P_i = O_{i-1} - B^a_{i-1,i} = O_{i-1}[1 - \frac{B^a_{i-1,i}}{O_{i-1}}] \tag{A.19}$$

$$N_i = O_i - P_i = O_i + B^a_{i-1,i} - O_{i-1} \quad \text{(A.20)}$$

The propagated delay in (A.19) can be similarly decomposed by root node as in (A.13) and (A.14).

Case 2(d): $O_i < O_{i-1}$ and $B_{i-1,i} > O_{i-1}$

In this case, buffer on link $(i-1, i)$ entirely eliminates propagated delay from upstream of node i (i.e., O_{i-1}). The observed delay at node i, O_i, is purely newly formed delay. Because $B_{i-1,i} > O_{i-1}$, an amount of buffer equal to $B_{i-1,i} - O_{i-1}$ will be used to absorbed newly formed delay. The expressions for P_i and N_i are exactly the same as in (A.16) and (A.17).

Appendix C: Estimation results

Table C.1: Model estimation results under scenario 1

Scenario 1	Departure node	Arrival node
Initiation		
Newly formed departure delay at node i	0.244***	
Newly formed arrival delay at node i		0.071***
Buffer on link $(i, i+1)$ $(B_{i,i+1})$	-0.020***	-0.0002***
Newly formed delay at node $i+1$ (N_{i+1})	0.029***	0.021***
Constant	-1.233***	-1.338***
Progression		
Newly formed departure delay at node i	0.932***	
Newly formed arrival delay at node i		0.176***
Propagated delay to node i $(\sum_{k=1}^{i-1} p_{k,i})$	0.064***	0.045***
Ground buffer in time group 1	-0.058***	-0.033***
Ground buffer in time group 2	-0.042***	-0.041***
Ground buffer in time group 3	-0.006***	-0.014***
Ground buffer in time group 4	-0.003***	-0.004***
Flight buffer in time group 1	-0.032***	0.003
Flight buffer in time group 2	0.008	-0.002
Flight buffer in time group 3	0.034***	-0.008
Flight buffer in time group 4	0.042***	-0.012***
Delay_6	0.135***	-0.083***
Delay_7	0.057***	0.024*
Delay_8	0.076**	0.043
Delay_9	0.140***	0.091***
Delay_10	0.067***	0.037*
Delay_11	0.164***	0.011
Delay_12	0.224***	0.108***
Delay_13	0.168***	0.101***
Delay_14	0.156***	0.134***
Delay_15	0.207***	0.141***
Delay_16	0.209***	0.112***
Delay_17	0.237***	0.115***
Delay_18	0.224***	0.088***
Delay_19	0.199***	0.094***
Delay_20	0.141***	0.073***
Delay_21	0.084***	0.052***
Constant	4.645***	36.634***
Observations	414,150	383,213
ρ	-0.46	-1.00
σ_ε	14.52	22.29
β_λ	-6.69	-22.29

*** significant at 1% level; ** significant at 5% level; * significant at 10% level.

Note: node i refers to the node based on which the observation unit is identified.

Table C.2: Model estimation results under scenario 2

Scenario 2	Departure node	Arrival node
Initiation		
Newly formed departure delay at node i	0.262***	
Newly formed arrival delay at node i		0.060***
Buffer on link $(i, i+1)$ $(B_{i,i+1})$	-0.202***	-0.023***
Propagated delay to node i $(\sum_{k=1}^{i-1} p_{k,i})$	0.153***	0.025***
Constant	-1.022***	-1.362***
Progression		
Newly formed departure delay at node i	0.883***	
Newly formed arrival delay at node i		-0.683***
Propagated delay to node i $(\sum_{k=1}^{i-1} p_{k,i})$	0.220***	-0.351***
Ground buffer in time group 1	-0.042***	-0.060***
Ground buffer in time group 2	-0.046***	-0.041***
Ground buffer in time group 3	-0.008***	-0.013***
Ground buffer in time group 4	-0.005***	-0.005
Flight buffer in time group 1	-0.145***	0.001
Flight buffer in time group 2	-0.189***	-0.036**
Flight buffer in time group 3	-0.076***	-0.013
Flight buffer in time group 4	-0.088***	-0.035***
Delay_6	0.034	-0.072
Delay_7	0.429***	0.001
Delay_8	0.240***	-0.085
Delay_9	0.342***	-0.033
Delay_10	0.320***	0.065
Delay_11	0.340***	0.062
Delay_12	0.394***	0.076**
Delay_13	0.362***	0.092***
Delay_14	0.333***	0.072**
Delay_15	0.336***	0.100***
Delay_16	0.317***	0.062**
Delay_17	0.271***	0.055**
Delay_18	0.294***	0.067***
Delay_19	0.241***	0.072***
Delay_20	0.170***	0.056***
Delay_21	0.115***	0.047***
Constant	-8.557***	83.924***
Observations	412747	383029
ρ	-0.22	-1.00
σ_ε	11.60	50.81
β_λ	-2.59	-50.81

*** significant at 1% level; ** significant at 5% level; * significant at 10% level.
Note: node i refers to the node based on which the observation unit is identified.

Table C.3: Model estimation results under scenario 3

Scenario 3	Departure node	Arrival node
Initiation		
Newly formed departure delay at node i	0.244***	
Newly formed arrival delay at node i		0.066***
Buffer on link $(i, i+1)$ $(B_{i,i+1})$	-0.030***	-0.001***
Propagated delay to node i $(\sum_{k=1}^{i-1} p_{k,i})$	0.034***	0.019***
Newly formed delay at node $i+1$ (N_{i+1})	0.057***	0.053***
Constant	-1.298***	-1.408***
Progression		
Newly formed departure delay at node i	0.767***	
Newly formed arrival delay at node i		0.463***
Propagated delay to node i $(\sum_{k=1}^{i-1} p_{k,i})$	0.084***	0.005
Ground buffer in time group 1	-0.006**	-0.047***
Ground buffer in time group 2	-0.013***	-0.061***
Ground buffer in time group 3	-0.003***	-0.024***
Ground buffer in time group 4	-0.002***	-0.016***
Flight buffer in time group 1	-0.057***	-0.005
Flight buffer in time group 2	-0.066***	0.003
Flight buffer in time group 3	-0.034***	0.000
Flight buffer in time group 4	-0.032***	-0.013***
Delay_6	0.084***	-0.135***
Delay_7	0.135***	-0.025
Delay_8	0.092***	-0.024
Delay_9	0.126***	0.017
Delay_10	0.126***	0.017
Delay_11	0.144***	0.023**
Delay_12	0.159***	0.077***
Delay_13	0.132***	0.070***
Delay_14	0.110***	0.086***
Delay_15	0.129***	0.102***
Delay_16	0.123***	0.072***
Delay_17	0.135***	0.074***
Delay_18	0.119***	0.081***
Delay_19	0.104***	0.084***
Delay_20	0.080***	0.057***
Delay_21	0.059***	0.043***
Constant	-1.530***	13.136***
Observations	385,214	358,219
ρ	-0.16	-0.88
σ_ε	5.82	10.41
β_λ	-0.95	-9.18

*** significant at 1% level; ** significant at 5% level; * significant at 10% level.
Note: node i refers to the node based on which the observation unit is identified.

References

1. AhmadBeygi S., Cohn A., Guan Y., Belobaba P., 2008. Analysis of the potential for delay propagation in passenger airline networks. Journal of Air Transport Management 14 (5), 221-236.
2. AhmadBeygi S., Cohn A., Lapp M., 2010. Decreasing airline delay propagation by re-allocating scheduled slack. IIE Transactions 42 (7), 478-489.
3. Arikan M., Deshpande V., Sohoni M., 2013. Building reliable air-travel infrastructure using stochastic models of airline networks. Operations Research 61 (1), 45-64.
4. Ball, M., Barnhart, C., Nemhauser, G. and Odoni, A., 2007. Air transportation: Irregular operations and control. Handbooks in operations research and management science 14, 1-67.
5. Ball, M., Barnhart, C., Dresner, M., Hansen, M., Neels, K., Odoni, A., Peterson, E., Sherry, L., Trani, A., Zou, B., 2010. Total delay impact study: a comprehensive assessment of the costs and impacts of flight delay in the United States. Research Report for the US Federal Aviation Adiminstration.
6. Barrat, A., Barthelemy, M., Pastor-Satorras, R., Vespignani, A., 2004. The architecture of complex weighted networks. Proceedings of the National Academy of Sciences 101 (11), 3747-3752.
7. Baumgarten, P., Malina, R., Lange, A., 2014. The impact of hubbing concentration on flight delays within airline networks: An empirical analysis of the US domestic market. Transportation Research Part E: Logistics and Transportation Review 66, 103-114.
8. Beatty, R., Hsu, R., Berry, L., Rome, J., 1999. Preliminary evaluation of flight delay propagation through an airline schedule. Air Traffic Control Quarterly 7 (4), 259–270.
9. Bureau of Transportation Statistics (BTS), 2013 a. Airline On-Time Performance. [Online] Available at: http://www.transtats.bts.gov/Tables.asp?DB_ID=120. Accessed on Nov. 25, 2013.
10. Campanelli, B., Fleurquin, P., Arranz, A., Etxebarria, I., Ciruelos, C., Eguíluz, V.M., Ramasco, J.J., 2016. Comparing the modeling of delay propagation in the US and European air traffic networks. Journal of Air Transport Management, in press.
11. Churchill, A., Lovell, D., Ball, M., 2010. Flight delay propagation impact on strategic air traffic flow management. Transportation Research Record: Journal of the Transportation Research Board 2177, 105-113.
12. Federal Aviation Administration (FAA), 2013 b. On-Time: Schedule B-43 Inventory. [Online] Available at: http://www.transtats.bts.gov/DL_SelectFields.asp?Table_ID=314. Accessed on Nov. 25, 2013.
13. Fleurquin, P., Ramasco, J.J., Eguiluz, V.M., 2013. Systemic delay propagation in the US airport network. Nature Scientific Reports 3, 1-6.
14. Greene, W., 2012. Econometric Analysis (7th Edition). Prentice Hall, New Jersey.
15. Guimerà, R., Mossa, S., Turtschi, A., Amaral, L.N., 2005. The worldwide air transportation network: Anomalous centrality, community structure, and cities' global roles. Proceedings of the National Academy of Sciences, 102 (22), 7794-7799.
16. Hao, L., Hansen M., 2014. Block time reliability and scheduled block time setting. Transportation Research Part B: Methodological 69, 98-111.
17. Johnson, N., Kotz, S., Distributions in Statistics – Continuous Multivariate Distributions (2nd Edition). Wiley and Sons, New York.
18. Martin J.C., Voltes-Dorta, A., 2009. A note on how to measure hubbing practices in airline networks. Transportation Research Part E: Logistics and Transportation Review 45 (1), 250-254.
19. Pyrgiotis N., Malone K.M., Odoni A., 2013. Modelling delay propagation within an airport network. Transportation Research Part C, Emerging Technologies 27, 60-75.
20. Schaefer, L., Millner D., 2001. Flight delay propagation analysis with the detailed policy assessment tool. Proceedings of the IEEE International Conference on Systems, Man, and Cybernetics 2, 1299-1303.
21. Schellekens B., 2011. Stochastic simulation of delay propagation: improving schedule stability at Kenya Airways. Master Thesis, Delft University of Technology.

22. Swaroop, P., Zou, B., Ball, M., Hansen, M., 2012. Do more U.S. airports need slot controls? A welfare based approach to determine slot levels. Transportation Research Part B: Methodological 46 (9), 1239-1259.
23. Welman, S., Williams, A., Hechtman, D., 2010. Calculating delay propagation multipliers for cost-benefit analysis. Research Report prepared by the Center for Advanced Aviation System Development (MITRE), MP 100039.
24. Wong J.T., Tsai S.C., 2012. A survival model for flight delay propagation. Journal of Air Transport Management 23, 5-11.
25. Xu, N., Sherry, L., Laskey, K., 2008. Multi-factor model for predicting delays at U.S. airports. Transportation Research Record: Journal of the Transportation Research Board 2052, 62-71.
26. Zou, B., Hansen, M., 2012a. Flight delays, capacity investment and social welfare under air transport supply-demand equilibrium. Transportation Research Part A: Policy and Practice 46 (6), 965-980.
27. Zou, B., Hansen, M., 2012b. Impact of operational performance on air carrier cost structure: evidence from US airlines. Transportation Research Part E: Logistics and Transportation Review 48, 1032-1048.
28. Zou, B., Elke, M., Hansen, M., Kafle, N., 2014. Evaluating air carrier fuel efficiency in the US airline industry. Transportation Research Part A: Policy and Practice 59, 306-330.
29. Zou, B., 2012. Flight delays, capacity investment and welfare under air transport supply-demand equilibrium. Ph.D. Dissertation, University of California at Berkeley.